

Short-Period Small Planets with High Mutual Inclinations are more Common around Metal-Rich Stars

XINYAN HUA ¹, SHARON XUESONG WANG ¹, DONGSHENG AN ^{2,3}, SONGHU WANG ⁴, YANG HUANG ^{5,6},
DICHANG CHEN ^{2,3}, JOHANNES BUCHNER ⁷, WEI ZHU ¹, FEI DAI ⁸, AND JIWEI XIE ^{2,3}

¹Department of Astronomy, Tsinghua University, Beijing 100084, China

²School of Astronomy and Space Science, Nanjing University, Nanjing 210023, China

³Key Laboratory of Modern Astronomy and Astrophysics, Ministry of Education, Nanjing 210023, China

⁴Department of Astronomy, Indiana University, 727 East 3rd Street, Bloomington, IN 47405-7105, USA

⁵School of Astronomy and Space Science, University of Chinese Academy of Sciences, Beijing 100049, China;

⁶Key Lab of Optical Astronomy, National Astronomical Observatories, Chinese Academy of Sciences, Beijing 100101, China

⁷Max-Planck-Institut für extraterrestrische Physik, Giessenbachstrasse 1, D-85748 Garching, Germany

⁸Institute for Astronomy, University of Hawai'i, 2680 Woodlawn Drive, Honolulu, HI 96822, USA

ABSTRACT

We present a correlation between the stellar metallicities and the mutual inclinations of multi-planet systems hosting short-period small planets ($a/R_\star < 12$, $R_p < 4 R_\oplus$). We analyzed 89 multi-planet systems discovered by *Kepler*, K2, and TESS, where the innermost planets have periods shorter than 10 days. We found that the mutual inclinations of the innermost two planets are higher and more diverse around metal-rich stars. The mutual inclinations are calculated as the absolute differences between the best-fit inclinations of the innermost two planets from transit modeling, which represent the lower limits of the true mutual inclinations. The mean and variance of the mutual inclination distribution of the metal-rich systems are $3.1^\circ \pm 0.5$ and $3.1^\circ \pm 0.4$, while for the metal-poor systems they are $1.3^\circ \pm 0.2$ and $1.0^\circ \pm 0.2$. This finding suggests that inner planetary systems around metal-rich stars are dynamically hotter. We summarized the theories that could plausibly explain this correlation, including the influence of giant planets, higher solid densities in protoplanetary disks around metal-rich stars, or secular chaos coupled with an excess of angular momentum deficits. Planet formation and population synthesis models tracking the mutual inclination evolution would be essential to fully understand this correlation.

1. INTRODUCTION

The angle between the orbital planes of planets, the mutual inclination, is an important proxy for studying the architecture of multi-planet systems. Mutual inclinations can offer valuable insights into planet formation and evolution history (e.g., Zhu & Dong 2021). Theoretically, inclined orbits can arise through various mechanisms, such as gravitational scattering of planetary embryos (Hansen & Murray 2013; Moriarty & Ballard 2016; Izidoro et al. 2021) or from gravitational perturbations like distant giant planets (Mustill et al. 2017; Lai & Pu 2017; Pu & Lai 2018). Besides planet-planet interactions, the stellar oblateness of a tilted star can induce differential nodal precession among coplanar planets,

potentially exciting mutual inclinations after the protoplanetary disk has dissipated (Millholland et al. 2021).

However, mutual inclinations are challenging to measure in practice for the majority of the exoplanet detection methods commonly used today (Zhu & Dong 2021). In principle, one can infer inclinations using the transit method or astrometry, but the transit method is heavily biased toward coplanar systems, while astrometry is primarily sensitive to objects several AU away and requires an extended time baseline to achieve sufficient accuracy.

Planets with short orbital periods provide a unique opportunity to investigate mutual inclinations, as their proximity to the host star results in a high chance of transit, even for highly inclined orbits. Dai et al. (2018) analyzed approximately 100 systems hosting short-period planets and concluded that short-period planets with $a/R_\star < 5$ (a , orbital semi-major axis; R_\star , stellar radius) are more mutually inclined. This suggests

that the processes responsible for shrinking these orbits also excite their inclinations, implying that these short-period planets have undergone dynamically chaotic, or “hot”, evolution processes.

Recent studies indicate that dynamically hot systems preferentially reside around metal-rich stars (e.g., see review by [Drażkowska et al. 2023](#)). Numerous works have demonstrated that giant planets are more common around metal-rich hosts (e.g., [Fischer & Valenti 2005](#); [Johnson et al. 2010](#); [Buchhave et al. 2012](#); [Chen et al. 2023](#)), particularly those with eccentric orbits ([Dawson & Murray-Clay 2013](#); [Buchhave et al. 2018](#)). A similar preference for metal-rich stars also exists for small planets in occurrence rate ([Wang & Fischer 2015](#); [Zhu 2019](#)) and orbital eccentricity ([Mills et al. 2019](#); [An et al. 2023](#)). [An et al. \(2023\)](#) found a positive correlation between metallicity and system-averaged mutual inclinations using the Transit Duration Ratio (TDR) method. In contrast, evidence suggests that compact multi-planet systems, which are generally more aligned (e.g., [Weiss et al. 2018](#)), tend to be around metal-poor stars ([Brewer et al. 2018](#); [Anderson et al. 2021](#)). This implies that metal-poor systems might be dynamically cooler.

In this paper, we report the correlation between mutual inclinations of the innermost two planets and stellar metallicities for short-period small planets ($a/R_\star < 12$, $R < 4 R_\oplus$), combining a sample of *Kepler* ([Borucki et al. 2010](#)) and TESS (Transiting Exoplanet Survey Satellite, [Ricker et al. 2015](#)) discoveries and enabled by uniform catalogs of stellar metallicities. This paper is organized as follows: Section 2 describes the sample selection process; Section 3 introduces our sources of stellar parameters; Section 4 details the photometric analyses to estimate mutual inclinations; and Section 5 reports our main findings and conclusions, followed by a discussion in Section 6.

2. SAMPLE SELECTION

We started with the sample from [Dai et al. \(2018\)](#), in which they selected transiting short-period planets from *Kepler* and K2 and conducted their own photometry analyses to determine planet properties. Specifically, [Dai et al. \(2018\)](#) required the apparent *Kepler* magnitude $K_p < 14$ mag, and the innermost planet to have a radius smaller than $4 R_\oplus$, an $a/R_\star < 12$, and a transit signal-to-noise ratio $S/N > 20$. The limit on $a/R_\star = 12$ corresponds to an allowed range of inclinations of $85 - 90^\circ$. We selected 94 systems with $a/R_\star < 12$ among the total 102 systems with innermost planets’ $a/R_\star < 20$ in their sample. We further excluded two systems, KOI-1239 and EPIC 211305568, as these were classified as planet candidates which have

not been confirmed according to the NASA Exoplanet Archive¹ (hereafter, NEA), resulting in a final set of 92 systems.

We expanded the [Dai et al. \(2018\)](#) sample by adding TESS targets. We applied the same selection criteria to the confirmed TESS multi-transiting systems from NEA, which resulted in an addition of 18 systems. We did not apply magnitude or S/N cuts to our TESS sample, as TESS targets are generally brighter than *Kepler* stars (e.g. [Guerrero et al. 2021](#)), and they are all confirmed planets with comparable error bars in the measured inclinations to the [Dai et al. \(2018\)](#) sample. The faintest target in our sample, LP 791-18, has a TESS magnitude of 13.6, with the second faintest at 12.3 and all others brighter than 11.

Finally, we restricted the size of the second innermost planets to be smaller than $4 R_\oplus$ to exclude giant planets in the inner system and focus on the mutual inclinations between small planets.² As a result, we selected a total of 89 systems for this study, consisting of 75 *Kepler* and K2 systems and 14 TESS systems. We modeled the light curves of the TESS targets to derive the best-fit orbital parameters (Section 4). For the TESS sample, the minimum value of a/R_\star is about 2.55, which corresponds to a Δi up to 21 degrees.

For both the [Dai et al. \(2018\)](#) and TESS samples, we derived the mutual inclination (Δi) between the innermost two planets in each system using their best-fit orbital inclinations, assuming they have parallel transit chords going across the same stellar hemisphere, i.e. $\Delta i = |i_1 - i_2|$. This results in the lower limit of the mutual inclination between the two planets (Section 6.3). Table 1 summarizes the information on these systems with an illustration in Figure 1.

Table 1. Summary of the sample information

Host	[Fe/H] (dex)	Δi ($^\circ$)	Origin of [Fe/H]
EPIC 206024342	$-0.255^{+0.011}_{-0.011}$	$3.95^{+3.05}_{-3.06}$	APOGEE
EPIC 220674823	$0.08^{+0.006}_{-0.006}$	$6.31^{+4.02}_{-4.82}$	APOGEE
HD 3167	$0.114^{+0.01}_{-0.01}$	$2.04^{+1.46}_{-1.54}$	APOGEE

To be continued

¹ We used the Planetary Systems Composite Data Table, available at: <https://exoplanetarchive.ipac.caltech.edu/cgi-bin/TblView/nph-tblView?app=ExoTbls&config=PSCompPars>, accessed on Mar. 8, 2024.

² Beyond the innermost two planets, there are 6 systems in our sample known to have planets larger than $4 R_\oplus$ but all smaller than $6.2 R_\oplus$ (mostly between $4-5 R_\oplus$) except for Kepler-1131 d ($R \sim 9.7 R_\oplus$). Removing these systems does not affect our conclusions.

Host	[Fe/H] (dex)	Δi ($^{\circ}$)	Origin of [Fe/H]	Host	[Fe/H] (dex)	Δi ($^{\circ}$)	Origin of [Fe/H]
K2-183	0.078 ^{+0.025} _{-0.025}	4.19 ^{+3.93} _{-3.27}	LAMOST	Kepler-342	0.147 ^{+0.043} _{-0.043}	0.85 ^{+1.19} _{-0.58}	PASTEL
K2-187	0.273 ^{+0.032} _{-0.032}	5.42 ^{+1.78} _{-2.6}	LAMOST	Kepler-356	0.037 ^{+0.053} _{-0.053}	1.8 ^{+0.3} _{-0.32}	PASTEL
K2-223	0.17 ^{+0.01} _{-0.01}	14.72 ^{+1.5} _{-2.11}	SWEET-Cat	Kepler-363	0.422 ^{+0.043} _{-0.043}	4.09 ^{+1.36} _{-1.06}	PASTEL
K2-229	0.123 ^{+0.025} _{-0.025}	1.84 ^{+2.26} _{-1.28}	LAMOST	Kepler-376	-0.1 ^{+0.053} _{-0.053}	0.8 ^{+0.97} _{-0.6}	PASTEL
K2-266	0.135 ^{+0.029} _{-0.029}	12.67 ^{+0.68} _{-0.75}	LAMOST	Kepler-380	-0.16 ^{+0.103} _{-0.103}	1.1 ^{+1.54} _{-0.78}	PASTEL
Kepler-10	-0.139 ^{+0.052} _{-0.052}	5.82 ^{+0.16} _{-0.17}	PASTEL	Kepler-381	-0.187 ^{+0.053} _{-0.053}	2.77 ^{+1.44} _{-1.81}	PASTEL
Kepler-100	0.107 ^{+0.036} _{-0.036}	1.66 ^{+0.46} _{-0.36}	LAMOST	Kepler-392	-0.355 ^{+0.03} _{-0.03}	0.78 ^{+0.77} _{-0.52}	PASTEL
Kepler-1047	0.285 ^{+0.07} _{-0.07}	6.3 ^{+3.55} _{-2.84}	PASTEL	Kepler-402	-0.05 ^{+0.023} _{-0.023}	0.77 ^{+0.74} _{-0.5}	PASTEL
Kepler-1067	0.213 ^{+0.053} _{-0.053}	6.75 ^{+1.67} _{-2.6}	PASTEL	Kepler-403	0.093 ^{+0.023} _{-0.023}	0.56 ^{+0.63} _{-0.4}	PASTEL
Kepler-107	0.275 ^{+0.043} _{-0.043}	1.62 ^{+0.8} _{-0.94}	PASTEL	Kepler-406	0.289 ^{+0.025} _{-0.025}	1.02 ^{+0.97} _{-0.77}	LAMOST
Kepler-116	0.07 ^{+0.057} _{-0.057}	0.71 ^{+1.71} _{-0.59}	PASTEL	Kepler-42	-0.5 ^{+0.09} _{-0.09}	2.95 ^{+0.6} _{-0.77}	Mann2017 ²
Kepler-1311	0.057 ^{+0.053} _{-0.053}	1.53 ^{+1.6} _{-1.03}	PASTEL	Kepler-431	-0.013 ^{+0.043} _{-0.043}	0.9 ^{+1.13} _{-0.65}	PASTEL
Kepler-1322	-0.07 ^{+0.151} _{-0.184}	2.1 ^{+1.89} _{-1.5}	Morton2016 ¹	Kepler-450	0.21 ^{+0.065} _{-0.065}	0.99 ^{+0.38} _{-0.4}	PASTEL
Kepler-135	-0.05 ^{+0.03} _{-0.03}	1.01 ^{+0.93} _{-0.71}	PASTEL	Kepler-466	-0.037 ^{+0.053} _{-0.053}	1.02 ^{+0.81} _{-0.71}	PASTEL
Kepler-1365	0.125 ^{+0.03} _{-0.03}	2.09 ^{+1.54} _{-0.95}	PASTEL	Kepler-524	0.01 ^{+0.03} _{-0.03}	1.65 ^{+1.82} _{-1.16}	PASTEL
Kepler-1371	-0.11 ^{+0.03} _{-0.03}	1.59 ^{+1.65} _{-1.08}	PASTEL	Kepler-60	-0.047 ^{+0.023} _{-0.023}	0.73 ^{+1.08} _{-0.53}	PASTEL
Kepler-1398	-0.073 ^{+0.083} _{-0.083}	1.45 ^{+1.29} _{-0.98}	PASTEL	Kepler-607	0.12 ^{+0.04} _{-0.04}	5.89 ^{+3.06} _{-3.96}	PASTEL
Kepler-140	-0.015 ^{+0.03} _{-0.03}	2.31 ^{+0.57} _{-1.06}	PASTEL	Kepler-625	0.173 ^{+0.053} _{-0.053}	3.34 ^{+1.08} _{-1.25}	PASTEL
Kepler-141	0.345 ^{+0.025} _{-0.025}	0.52 ^{+0.53} _{-0.36}	PASTEL	Kepler-653	0.283 ^{+0.053} _{-0.053}	12.38 ^{+1.52} _{-1.72}	PASTEL
Kepler-142	0.037 ^{+0.057} _{-0.057}	0.89 ^{+0.81} _{-0.62}	PASTEL	Kepler-732	-0.029 ^{+0.008} _{-0.008}	1.71 ^{+0.55} _{-0.67}	APOGEE
Kepler-1542	0.055 ^{+0.043} _{-0.043}	1.77 ^{+1.88} _{-1.34}	PASTEL	Kepler-755	0.04 ^{+0.07} _{-0.07}	1.58 ^{+2.67} _{-1.07}	PASTEL
Kepler-1814	0.13 ^{+0.03} _{-0.03}	2.27 ^{+1.46} _{-1.49}	PASTEL	Kepler-80	0.065 ^{+0.055} _{-0.055}	0.89 ^{+0.9} _{-0.65}	PASTEL
Kepler-1834	-0.057 ^{+0.053} _{-0.053}	5.59 ^{+1.3} _{-1.86}	PASTEL	Kepler-865	0.3 ^{+0.12} _{-0.12}	3.91 ^{+2.33} _{-2.69}	PASTEL
Kepler-197	-0.398 ^{+0.043} _{-0.043}	0.35 ^{+0.45} _{-0.24}	PASTEL	Kepler-969	0.13 ^{+0.03} _{-0.03}	0.82 ^{+0.96} _{-0.6}	PASTEL
Kepler-198	0.065 ^{+0.06} _{-0.06}	2.43 ^{+1.41} _{-1.91}	PASTEL	Kepler-990	-0.103 ^{+0.053} _{-0.053}	3.82 ^{+3.89} _{-2.96}	PASTEL
Kepler-20	0.096 ^{+0.058} _{-0.058}	0.2 ^{+0.35} _{-0.16}	LAMOST	HD 108236*	-0.302 ^{+0.011} _{-0.011}	1.18 ^{+0.67} _{-0.48}	SWEET-Cat
Kepler-203	0.083 ^{+0.09} _{-0.09}	3.39 ^{+1.18} _{-1.3}	PASTEL	HD 22946*	-0.085 ^{+0.015} _{-0.015}	0.12 ^{+0.97} _{-0.89}	SWEET-Cat
Kepler-207	0.28 ^{+0.023} _{-0.023}	5.93 ^{+1.91} _{-2.33}	PASTEL	HD 63433*	0.0 ^{+0.02} _{-0.02}	0.41 ^{+0.8} _{-0.88}	SWEET-Cat
Kepler-208	0.015 ^{+0.025} _{-0.025}	0.68 ^{+0.71} _{-0.43}	PASTEL	HD 93963 A*	0.1 ^{+0.04} _{-0.04}	0.77 ^{+0.99} _{-1.27}	SWEET-Cat
Kepler-213	0.16 ^{+0.053} _{-0.053}	0.94 ^{+0.37} _{-0.37}	PASTEL	HR 858*	-0.02 ^{+0.02} _{-0.02}	0.24 ^{+0.5} _{-0.62}	SWEET-Cat
Kepler-216	-0.06 ^{+0.03} _{-0.03}	0.65 ^{+0.59} _{-0.47}	PASTEL	LHS 1678*	-0.45 ^{+0.11} _{-0.11}	0.11 ^{+0.8} _{-0.95}	SWEET-Cat
Kepler-217	-0.033 ^{+0.023} _{-0.023}	3.53 ^{+1.52} _{-1.86}	PASTEL	LP 791-18*	-0.09 ^{+0.19} _{-0.19}	0.08 ^{+0.91} _{-0.89}	Peterson2023 ³
Kepler-218	0.335 ^{+0.055} _{-0.055}	0.8 ^{+0.81} _{-0.58}	PASTEL	LTT 3780*	0.06 ^{+0.11} _{-0.11}	3.27 ^{+0.63} _{-0.56}	Bonfanti2024 ⁴
Kepler-219	0.36 ^{+0.043} _{-0.043}	1.85 ^{+0.36} _{-0.43}	PASTEL	TOI-1260*	-0.1 ^{+0.07} _{-0.07}	0.92 ^{+0.46} _{-0.36}	Lam2023 ⁵
Kepler-221	0.01 ^{+0.03} _{-0.03}	0.98 ^{+0.51} _{-0.51}	PASTEL	TOI-1749*	-0.347 ^{+0.014} _{-0.014}	2.11 ^{+0.54} _{-0.46}	APOGEE
Kepler-232	0.3 ^{+0.1} _{-0.1}	7.55 ^{+4.07} _{-5.61}	PASTEL	TOI-178*	-0.393 ^{+0.053} _{-0.053}	0.43 ^{+0.97} _{-0.94}	SWEET-Cat
Kepler-290	-0.1 ^{+0.04} _{-0.04}	5.23 ^{+2.37} _{-3.28}	PASTEL	TOI-431*	0.02 ^{+0.08} _{-0.08}	3.85 ^{+1.51} _{-1.48}	PASTEL
Kepler-312	0.2 ^{+0.053} _{-0.053}	9.12 ^{+1.19} _{-1.38}	PASTEL	TOI-451*	-0.025 ^{+0.019} _{-0.019}	0.41 ^{+0.99} _{-1.09}	SWEET-Cat
Kepler-314	0.32 ^{+0.05} _{-0.05}	0.79 ^{+0.73} _{-0.52}	PASTEL	TOI-561*	-0.378 ^{+0.008} _{-0.008}	1.34 ^{+1.32} _{-1.64}	APOGEE
Kepler-32	-0.5 ^{+0.32} _{-0.32}	1.64 ^{+1.33} _{-1.16}	PASTEL				
Kepler-322	0.083 ^{+0.053} _{-0.053}	2.12 ^{+0.92} _{-1.21}	PASTEL				
Kepler-323	-0.173 ^{+0.053} _{-0.053}	0.82 ^{+1.01} _{-0.55}	PASTEL				
Kepler-326	0.19 ^{+0.025} _{-0.025}	3.59 ^{+1.36} _{-1.51}	PASTEL				
Kepler-33	0.122 ^{+0.066} _{-0.066}	0.76 ^{+1.02} _{-0.53}	PASTEL				
Kepler-335	0.34 ^{+0.07} _{-0.07}	4.54 ^{+0.34} _{-0.31}	PASTEL				
Kepler-337	0.06 ^{+0.053} _{-0.053}	2.16 ^{+1.27} _{-1.31}	PASTEL				
Kepler-338	-0.02 ^{+0.056} _{-0.056}	1.0 ^{+0.58} _{-0.66}	PASTEL				

To be continued

* Mutual inclinations measured from this work.

¹Morton et al. (2016)

²Mann et al. (2017)

³Peterson et al. (2023)

⁴Bonfanti et al. (2024)

⁵Lam et al. (2023)

3. STELLAR PARAMETERS

We collected the stellar properties for our targets by cross-matching the samples with the Planetary Systems Composite Data table from NEA, in particular, the metallicity, $[\text{Fe}/\text{H}]$, and mass of each host star. However, these measurements come from various publications and are thus heterogeneous. In order to minimize biases that may arise from different methods of estimating $[\text{Fe}/\text{H}]$, we searched for $[\text{Fe}/\text{H}]$ values for our targets across various databases of stellar parameters, including LAMOST (The Large Sky Area Multi-Object Fiber Spectroscopic Telescope, Cui et al. 2012), APOGEE (Apache Point Observatory Galactic Evolution Experiment, Holtzman et al. 2018), SWEET-Cat (Sousa et al. 2021) and PASTEL (Soubiran et al. 2016).

Briefly, PASTEL compiles atmospheric parameters (effective temperature T_{eff} , surface gravity $\log g$, and $[\text{Fe}/\text{H}]$) from high-resolution, high-S/N spectra for over 18,000 stars with $[\text{Fe}/\text{H}]$ precision better than 0.05 dex for stars with $[\text{Fe}/\text{H}] > -2.0$, as noted by Huang et al. (2022). SWEET-Cat provides homogeneously derived spectroscopic parameters and utilizes Gaia eDR3 parallaxes to improve surface gravity precision, thus enhancing the reliability of the catalog’s stellar parameters. The LAMOST and APOGEE catalogs are commonly used for exoplanet demographic studies as their parameters are uniformly derived using data from large spectroscopic surveys (e.g., Xie et al. 2016).

We cross-matched our sample with these databases and found 67 matches in PASTEL, 52 in LAMOST, 43 in APOGEE, and 21 in SWEET-Cat. Figure 2 compares the $[\text{Fe}/\text{H}]$ values of the cross matches from each database with the literature values listed on NEA. Among the databases, PASTEL showed no significant bias or offset compared to the uniform databases (LAMOST and APOGEE) and covered the most targets in our sample. Therefore, we prioritized using the $[\text{Fe}/\text{H}]$ from these databases as follows: PASTEL > LAMOST > APOGEE > SWEET-Cat > Literature, favoring results from high-resolution spectroscopy (PASTEL). We also verified that our conclusion remained if we primarily adopted the metallicities from the uniform catalogs (LAMOST and APOGEE).

In addition, we have five targets using $[\text{Fe}/\text{H}]$ values from the literature as they are not covered by the databases listed above. We have also verified that our main conclusion (next section) does not depend on the specific choice or prioritization of $[\text{Fe}/\text{H}]$ values, as long as they are mostly from these databases. We list the metallicities of the 89 targets in our sample and their origins in Table 1.

4. MUTUAL INCLINATIONS FROM TESS PHOTOMETRY

We performed fitting to the light curves of the 14 TESS systems to ensure a homogeneous analysis in deriving Δi , similar to Dai et al. (2018), and we describe our fittings in this section. We downloaded all available light curves with 2-min exposures for the TESS targets reduced by the Science Processing Operations Center (SPOC; Jenkins et al. 2016) from the Mikulski Archive for Space Telescopes³ (MAST) using the python package `lightkurve` (Lightkurve Collaboration et al. 2018). We used the Presearch Data Conditioning Simple Aperture Photometry light curve files (PDCSAP flux; Stumpe et al. 2012; Smith et al. 2012; Stumpe et al. 2014), which were extracted using Simple Aperture Photometry (SAP) and calibrated for instrument systematics by the Presearch Data Conditioning (PDC) algorithm.

We first detrended the light curves using the Gaussian Process (GP) models with the Matern 3/2 kernel, and all transit windows were masked according to the transit epochs and periods from the literature. We set uninformative priors for the GP with wide bounds for most parameters. We examined the detrended light curves and identified two systems around active stars, HD 63433 and TOI-451. We further processed their light curves to eliminate the stellar flares by removing data points beyond the 2.5–3 σ range of a smoothed version of the light curves before performing another round of detrending.

After detrending, we performed an initial transit fit using the `Juliet` package (Espinoza et al. 2019), accounting for all known transiting planets in each system. We assume Gaussian priors for the transit-time-center, $t_{0,i}$, and period, P_i , according to the best-fit values reported in the literature, with the standard deviation set to 1.5 times the transit duration. To simplify the initial model, we fixed eccentricities, e_i , and arguments of periapsis, ω_i , for all planets to zero and 90 degrees, respectively. The host star density, ρ_* , was assigned a normal distribution prior using the reported value and uncertainties from publications. All other stellar, planetary, or light curve systematic parameters were set to have uninformative priors (wide uniform or log-uniform distributions).

If the best-fit planetary parameter has a relatively large discrepancy (e.g. $> 1\sigma$) with the literature, we would adopt more informative priors for a second round of fitting in order to better constrain the orbital parameters. The specific adjustments on the priors vary

³ <https://archive.stsci.edu>

from target to target. For instance, we would narrow the priors of $t_{0,i}$ or period or planet-to-star radius ratio, or adopt the exact same priors as in the publications. We examined the best-fit phase-folded light curves to confirm that none of our systems has detectable TTVs.

Finally, we performed a model comparison between circular and eccentric orbit configurations. We used the parameterization of $\sqrt{e_i} \sin \omega_i$ and $\sqrt{e_i} \cos \omega_i$ with priors $\mathcal{U}(-0.6, 0.6)$ (a somewhat arbitrary value smaller than 1.0 for computational efficiency), corresponding to eccentricities ranging from 0 to 0.72. Only one system, TOI-451, showed a strong preference for the eccentric orbit model, with $\Delta(\log Z) = 51.5$. We then adopted the eccentric orbit model, though the mutual inclination remains consistent with the circular one within the uncertainty. The Δi values derived from the best-fit inclinations via $\Delta i = |i_1 - i_2|$ are listed in Table 1.

5. MUTUAL INCLINATION VS. METALLICITY

5.1. Main results

The stellar metallicity of the host star and the mutual inclinations, Δi , for the innermost two planets in each of the 89 systems in our sample are listed in Table 1. We emphasize that this Δi that calculated from $|i_1 - i_2|$ is the lower limit of the true mutual inclination (see discussion in Section 6.3).

The relation between Δi and $[\text{Fe}/\text{H}]$ is shown in Figure 3: systems with higher stellar metallicity tend to exhibit larger mutual inclinations. A Spearman correlation test yields a coefficient of 0.31 and a p -value of 0.0031, suggesting a moderate positive correlation between $[\text{Fe}/\text{H}]$ and Δi . However, a more prominent feature of this trend is that the distribution of mutual inclinations is more dispersed for metal-rich hosts. For a quantitative comparison, we divided the sample into metal-rich and metal-poor groups based on the median $[\text{Fe}/\text{H}]$ value of 0.055 dex, resulting in 45 metal-rich and 44 metal-poor systems. An Anderson-Darling (AD) test between these two groups yields a p -value of 0.0025, which indicates that they originate from distinct populations.

To further quantify the differences in the mutual inclination distributions between the metal-rich and metal-poor groups, we modeled the distribution of Δi using a β -distribution. We adopted β -distributions in our model because of its flexibility in shape (e.g., in comparison to the Rayleigh distribution; Lissauer et al. 2011). We show the best-fit β -distribution models in Figure 4, along with the posterior distributions of parameters, α , and β , and the derived mean (μ) and variance (σ) of Δi . The posteriors and Bayesian evidence were derived using the nested sampling Monte Carlo algorithm ML-

Friends (Buchner 2016, 2019), implemented through the UltraNest⁴ package (Buchner 2021). The algorithm considers heterogeneous and asymmetric uncertainties for each data point. As illustrated in Figure 4, the metal-rich (red) and metal-poor (blue) groups exhibit remarkably different Δi distributions. The metal-rich group shows a larger average Δi with $\mu = 3.13^{+0.51}_{-0.49}$, and a more spread distribution characterized by $\sigma = 3.12^{+0.43}_{-0.43}$. In contrast, the metal-poor group has $\mu = 1.30^{+0.20}_{-0.21}$ and $\sigma = 1.00^{+0.19}_{-0.19}$, both of which are significantly smaller. The Mann-Whitney U test (Mann & Whitney 1947) gives p -values $< 10^{-10}$ for both μ 's and σ 's posterior distributions, indicating that the means of the two distributions are significantly different.

5.2. Other effects

Stellar metallicity is related to stellar mass. We considered the correlation between stellar mass and Δi (right panel of Figure 5) and how this could affect the $[\text{Fe}/\text{H}]-\Delta i$ correlation. The stellar mass measurements were adopted directly from the NEA. At first glance, higher mass stars seem to host planets with higher Δi . However, the Spearman correlation test yields $r = -0.17$ and $p = 0.11$, and the AD test between the low- and high-mass group divided by the median mass ($1.0 M_{\odot}$, 44 in the sub-solar bin and 45 in the super-solar bin) of our sample gives $p = 0.15$, indicating low statistical significance. In addition, we performed the same β -distribution modeling to four sub-samples divided by the median $[\text{Fe}/\text{H}]$ and stellar mass, and we found that Δi varies more significantly along the metallicity dimension than the stellar mass one.

To further verify the effect from stellar mass, we employed the nearest neighbor method for a sample control test to decouple the correlation between Δi vs. stellar mass or metallicity, following a procedure similar to that of An et al. (2023). Specifically, we first selected a star from the metal-rich group and calculated its mass difference with each star in the metal-poor group. We then matched the metal-rich star with the two metal-poor stars with the smallest mass differences. This process was repeated for every star in the metal-rich group, resulting in a new subsample from the metal-poor group with a mass distribution closely resembling that of the metal-rich group. This approach allowed us to minimize the influence of stellar mass on the relationship between Δi and stellar metallicity. As a result, 33 stars were selected from the metal-poor group, creating a total subsample of 78 systems (left panel of Figure 5).

⁴ <https://johannesbuchner.github.io/UltraNest/>

A similar approach was applied to the subsample divided by stellar mass at the median value of $1.0 M_{\odot}$ to reduce the influence of metallicity (right panel of Figure 5). We selected 35 systems from the sub-solar mass group, resulting in a new subsample of 81 systems. The same tests were conducted on the new samples. The Spearman test indicated that the correlation between Δi and metallicity remains significant, with a p -value of 0.0028, and the AD test comparing the metal-rich and metal-poor subgroups yields a p -value of 0.0072. In contrast, for stellar mass, the Spearman and AD tests returned p -values of 0.02 and 0.089, respectively, indicating no significant evidence for a relationship between stellar mass and Δi . We conclude that the [Fe/H]- Δi correlation is the dominant one, although our sample cannot fully rule out an additional correlation between Δi and stellar mass. We also performed a similar parameter control on the stellar radius and arrived at the same conclusion.

Besides stellar mass, stellar metallicity is negatively correlated with stellar age (Bensby et al. 2014; Chen et al. 2021). However, the observed positive correlation between Δi and [Fe/H] is unlikely to be due to the metallicity-age correlation. Both theories (Zhou et al. 2007) and statistical studies (Yang et al. 2023) have shown that mutual inclinations increase with stellar age, which would predict a negative correlation between Δi and [Fe/H], contrary to what we observe here. Due to the limited number of samples with precise age measurements, parameter control cannot yet be effectively performed. Nevertheless, we expect that after correcting for the age effect, the observed positive correlation between the metallicity and mutual inclination will become stronger.

Finally, we address the selection bias in metal-rich systems, as the metal-rich stars have larger radii in general than the metal-poor stars in our sample. This results in higher transit probabilities for multi-planet systems and thus larger detectable Δi for the metal-rich stars. We calculated the maximum allowed mutual inclination, Δi_{max} ⁵, for each system. The Spearman test yields $p = 0.07$ between [Fe/H] and Δi_{max} , indicating a weak correlation (selection bias). We then performed a similar sample control on Δi_{max} to further reduce the selection bias on our sample, in which 82 systems were reselected. The [Fe/H]- Δi correlation remains significant with Spearman $p = 0.0061$ and AD test $p = 0.0079$. Best-fit β -distributions for the metal-

rich ([Fe/H] ≥ 0.0625 dex) and metal-poor bins are $\mu = 3.2^{\circ} \pm 0.6$, $\sigma = 3.2^{\circ} \pm 0.5$ and $\mu = 1.5^{\circ} \pm 0.2$, $\sigma = 1.1^{\circ} \pm 0.2$, respectively, consistent with the results from the original sample. This indicates that this selection bias does not significantly affect our conclusions.

6. DISCUSSION

6.1. Comparison with previous studies

An et al. (2023) identified a positive mutual inclination-metallicity trend after examining a sample of small *Kepler* planets/candidates with uniform [Fe/H] measurements from LAMOST. While our conclusion generally aligns with the finding in An et al. (2023), it is important to note that our study focuses on a different sample from theirs: our innermost planets all have $a/R_{\star} < 12$ and An et al. (2023) used a generic *Kepler* sample, with only 14% among 152 systems having the innermost planet with $a/R_{\star} < 12$. Furthermore, they calculated average mutual inclinations, $\overline{\Delta i}$, for entire planetary systems across metallicity bins in a probabilistic manner, whereas we derived Δi specifically between the innermost two planets. They used the mutual TDR as a proxy for mutual inclinations allowing more transit scenarios, which would lead to higher estimations on $\overline{\Delta i}$ than ours (see more in Section 6.3). However, Figure 13 in An et al. (2023) shows comparable mutual inclinations to ours, which means they would have derived lower values for Δi if adopting the same assumption as ours, i.e. the planets transit over the same stellar hemisphere (Section 2). Unfortunately, the uncertainties on the sample means are relatively large for both samples (both being $\sim 3^{\circ} \pm (1 \sim 2)^{\circ}$), making it hard to conclude quantitatively. Nonetheless, the general consistency between the two works lends confidence to the robustness of our results, although it is not clear yet whether the mutual inclination-metallicity trend in the short-period planet sample is an extension of the generic trend or a distinct one.

It is important to consider the metallicity-inclination correlation in tandem with orbital periods. Dai et al. (2018) observed that shorter-period planets tend to have higher mutual inclinations, while Petigura et al. (2018) and Mulders et al. (2016) reported that short-period planets ($P < 10$ days) are more common around metal-rich stars, which seems to suggest that the metallicity-inclination correlation reported here might be a projection of these two previously known correlations. We performed a test to show that this is not the case using a control sub-sample with orbital periods between 1–5 days, where the period-metallicity anti-correlation plateaus with the Spearman test yields $r = -0.05$ and $p = 0.73$, indicating no significant correlation between

⁵ $\Delta i_{max} = \arcsin(R_{\star}/a_1) + \arcsin(R_{\star}/a_2)$, where a_1 and a_2 are the semi-major axes of the innermost and second innermost planets.

periods and metallicities. For the 48 samples within this period range, the Spearman test yields $r = 0.32$, $p = 0.025$ between $[\text{Fe}/\text{H}]$ and Δi , and the AD test yields $p = 0.016$ between metal-rich and metal-poor bins divided by the mean $[\text{Fe}/\text{H}]$ (0.056 dex) of the sub-sample, which indicate a consistent positive correlation, suggesting that the $[\text{Fe}/\text{H}]$ - Δi correlation should be intrinsic rather than a projection.

In addition, we highlight that the mutual inclination-metallicity correlation is not driven by the presence of USPs in our sample for the following reasons: (1) There is no evidence suggesting that USPs are associated with more metal-rich stars compared to other short-period planets with $P = 1$ –10 days (Winn et al. 2017). In our sample, the mean metallicity of the USP hosts does not appear to be super-solar. (2) The systems with USPs as the innermost planets do have higher mutual inclinations in general, but the relation persists after removing all USPs ($P < 1$ day) from our sample, for which the Spearman correlation coefficient $r = 0.36$ with a p-value of 0.0042.

6.2. Possible theoretical explanations

The observed correlation among period, metallicity, and mutual inclination appears to favor a dynamically hot origin, similar to the formation of hot Jupiters.

One possibility is that the disks of metal-rich stars could harbor more solids, leading to the formation of more giant planets (e.g., Ida & Lin 2008; Mordasini et al. 2012; Ndugu et al. 2018). A mutually inclined distant giant can tilt the inner planets to inclined orbits via precession (e.g. Becker & Adams 2017; Lai & Pu 2017; Pu & Lai 2018, 2021) or alternatively through planet-planet scattering (e.g. Mustill et al. 2017). This picture seems to corroborate with the observational findings that super-Earths are often accompanied by outer giant planets (Zhu et al. 2018; Bryan et al. 2019), especially for metal-rich stars (Zhu 2024), but unfortunately, our sample does not have sufficient follow-up data to enable further investigation on the inner-outer correlation.

Without invoking the existence of giant planets, high metallicity could result in a higher pebble flux in the protoplanetary disk, raising the probability of forming resonant chains (Drażkowska et al. 2023). This will end up in dynamical instability once the gas disk disperses, leading to a more dynamically hot system with higher Δi and e in general (e.g., Izidoro et al. 2017; Lambrechts et al. 2019; Izidoro et al. 2021).

Alternatively, secular chaos may produce highly inclined innermost planets in mature planetary systems (and could also explain USP formation, as in Petrovich et al. 2019; Pu & Lai 2019). Secular interactions can

redistribute angular momentum deficit (AMD) and systems with more and higher-mass planets typically have greater AMD. Considering that metal-rich systems tend to host more diverse planets in terms of size and mass (Millholland et al. 2017; Petigura et al. 2018), this may explain why such dynamical excitation is correlated with stellar metallicity, especially for the innermost planets. However, forming inclined USPs through secular chaos typically requires widely spaced external planets (e.g. Petrovich et al. 2019; Becker et al. 2020), a configuration not well-matched by our sample (Figure 1). Future work on orbital architecture of these systems combined with additional simulations tracking the inclination evolution of short-period planets are needed to determine or rule out secular interactions as an explanation.

In addition to these mechanisms mentioned above, other perturbative processes may also excite mutual inclinations, such as those related to stellar oblateness (e.g., Spalding & Batygin 2016; Becker et al. 2020; Brejka & Becker 2021; Faridani et al. 2024) or stellar perturbers during disk phase (e.g., Zanazzi & Lai 2018), although it is less obvious how they could correlate with stellar metallicity. For a more thorough discussion on the various mechanisms that could generate inclined planet orbits, we refer the readers to Section 5 of Millholland et al. (2021).

6.3. Caveats

As mentioned in Section 2, our mutual inclination is estimated for the innermost two planets in each system assuming both planets transit the same stellar hemisphere. However, in practice, two transiting planets with identical impact parameters (inclinations) may transit across opposite hemispheres or have different ascending nodes, both resulting in non-zero mutual inclinations.

We argue that this caveat does not affect our main conclusion as following: (1) If two planets have inclinations of i_1 and i_2 (assuming $i_1 < i_2$ for simplicity as the result would be the same otherwise), Δi will increase by $2 \times (90 - i_1)$ if the other planet transits in the opposite hemisphere. The median inclination of the innermost planets in our sample is 87.2° , which would lead to an increase of 5.6 degrees in Δi . (2) If two planets have different ascending nodes, the true mutual inclination could be arbitrarily large, but this would require a special viewing angle to see both planets transiting and is thus relatively rare. Furthermore, since systems with both high and low mutual inclinations have an equal probability of increasing their Δi due to these effects, they should not impact our main conclusion that the metal-rich stars host systems with higher Δi on average. However, they would alter the quantified mean

and variance of Δi for the two populations, rendering the reported values in this paper the lower limits.

7. CONCLUSION AND FUTURE WORK

In this work, we studied 89 multi-planet systems with the innermost planets within 10 days and reported a positive trend between stellar metallicity, $[\text{Fe}/\text{H}]$, and mutual inclination, Δi , of the innermost two planets: short-period planets around metal-rich stars have larger and more diverse mutual inclinations. We considered the effect of stellar mass and age and concluded that metallicity is likely the dominant factor, though a connection to stellar mass cannot be entirely ruled out.

Future studies can further probe the origin of this correlation and test the theoretical explanations. For example, follow-up observations of high mutual inclination systems to confirm the presence or absence of additional non-transiting giant planets could be helpful, especially since the majority of the *Kepler* systems in our sample lack RV follow-up. More in-depth studies taking into account *Kepler* and TESS detection completeness and biases would yield better quantified intrinsic mutual inclination distributions. In addition, planetary population synthesis work often does not track inclinations or assumes coplanarity throughout. Therefore, we advocate for more theoretical and simulation works to target orbital inclinations and explore the origin and evolution of mutual inclinations in planetary systems.

X. Hua and S. X. Wang acknowledge support from NSFC grant 12273016 as well as Tsinghua Dushi Funding No. 53121000124. Work by W. Zhu is supported by NSFC grant (No. 12173021 and 12133005). X. Hua thanks Zhecheng Hu for his valuable suggestions on removing stellar flares. We thank Norm Murray and Sam Hadden for helpful discussions regarding theoretical interpretation. We acknowledge the use of public TESS data from pipelines at the TESS Science Office and at the TESS Science Processing Operations Center. Resources supporting this work were provided by the NASA High-End Computing (HEC) Program through the NASA Advanced Supercomputing (NAS) Division at Ames Research Center for the production of the SPOC data products. This paper includes data collected with the TESS mission, obtained from the MAST data archive at the Space Telescope Science Institute (STScI). Funding for the TESS mission is provided by the NASA Explorer Program. STScI is operated by the Association of Universities for Research in Astronomy, Inc., under NASA contract NAS 5–26555. All the TESS data used in this paper can be found in MAST: doi: [10.17909/ak7h-3z66](https://doi.org/10.17909/ak7h-3z66). This research has made use of the Exoplanet Follow-up Observation Program website, which is operated by the California Institute of Technology, under contract with the National Aeronautics and Space Administration under the Exoplanet Exploration Program (doi: [10.26134/ExoFOP3](https://doi.org/10.26134/ExoFOP3)). This research has made use of the NEA, which is operated by the California Institute of Technology, under contract with the National Aeronautics and Space Administration under the Exoplanet Exploration Program.

Software: `lightkurve` (Lightkurve Collaboration et al. 2018), `Juliet` (Espinoza et al. 2019), `dynesty` (Speagle 2019), `PyMultiNest` (Buchner et al. 2014), `UltraNest` (Buchner 2021).

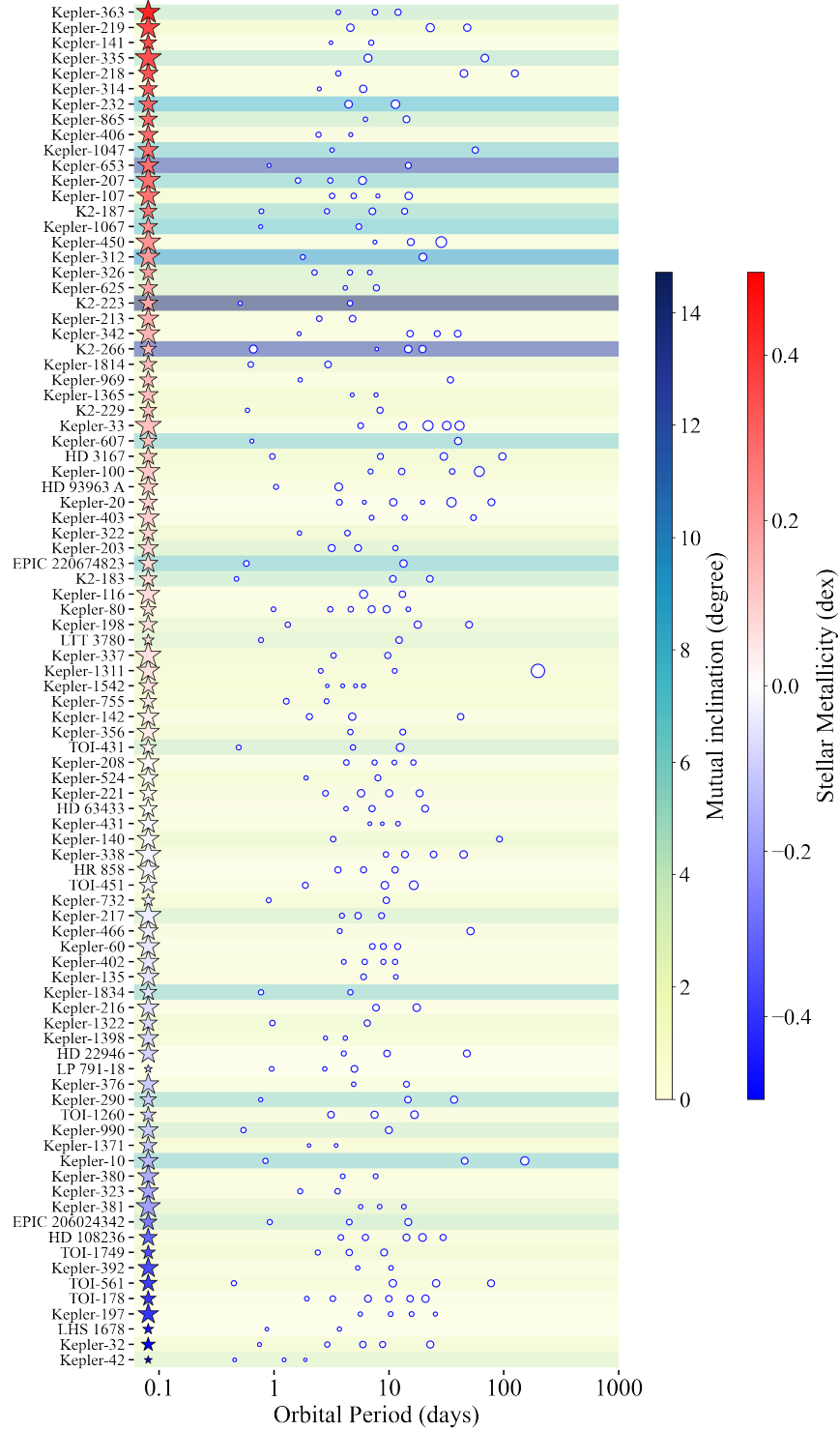


Figure 1. String plot for the 89 planetary systems in this work, with system names labeled on the left. Host stars are sorted and color-coded based on their $[Fe/H]$ values, with more metal-rich stars plotted on top with warmer colors. The background grids are shaded according to mutual inclinations, Δi , where darker shades correspond to higher values. The sizes of the star and planet symbols are scaled by their radii. $[Fe/H]$ and Δi values used to create this figure are listed in Table 1, while other parameters are from the NEA.

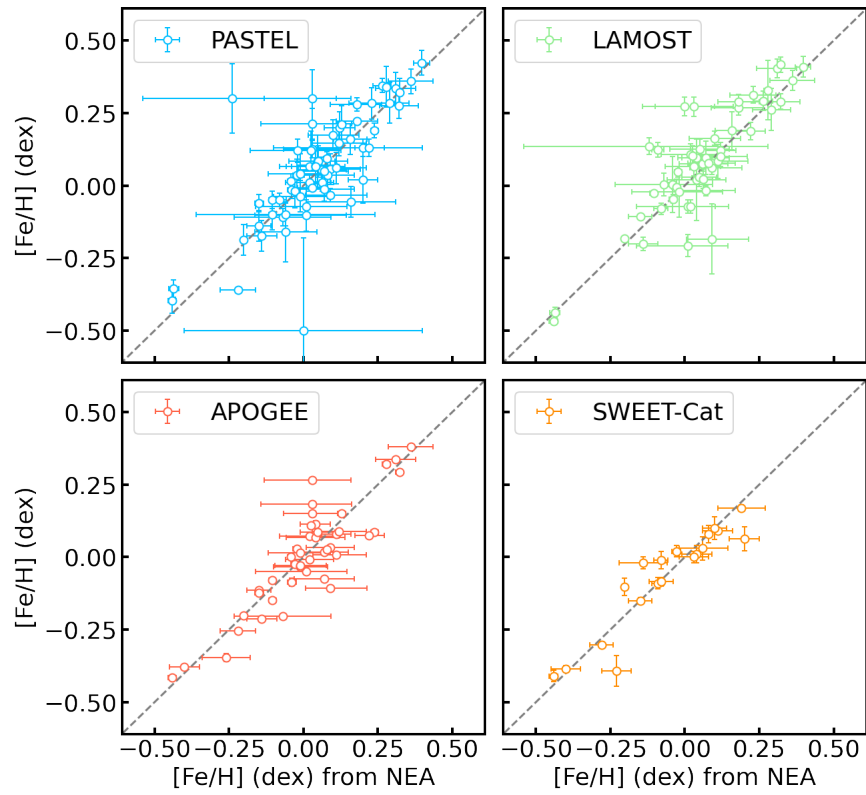


Figure 2. Comparison of stellar metallicity ($[\text{Fe}/\text{H}]$) between each database (y-axis) and the literature (x-axis) for overlapping systems in our sample. The measurements show good agreement with published data within the error bars, with no obvious offset or bias recognized.

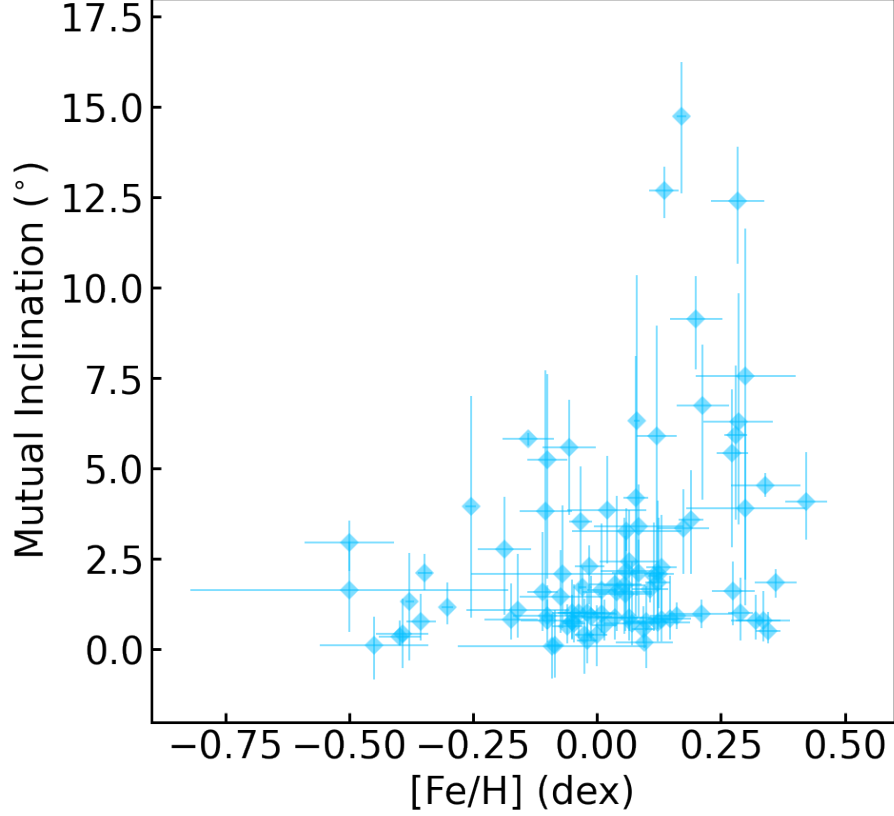


Figure 3. Stellar metallicity vs. mutual inclination plot. The mutual inclinations come from light curve fitting, and $[\text{Fe}/\text{H}]$ are carefully picked from multiple uniform databases (see Section 3). In total, we have 89 systems in our sample. We found that as stellar metallicity increases, the distribution of mutual inclination tends to be more spread.

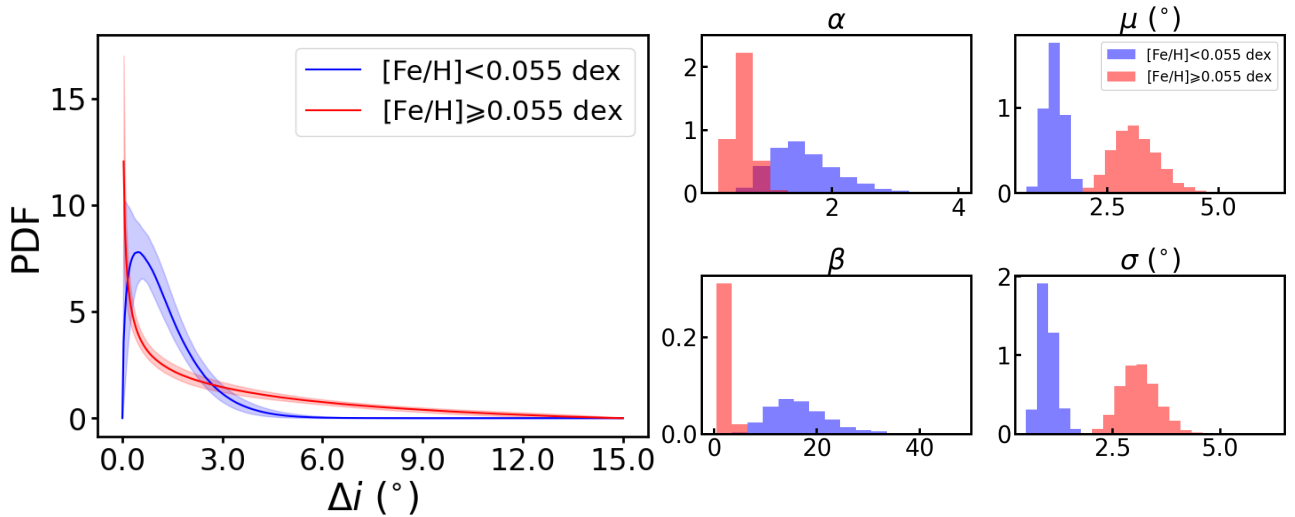


Figure 4. Distributions of Δi of metal-poor (blue) and metal-rich (red) samples modeled by β -distributions. The posterior distributions of the model parameters are attached on the right, where μ is the mean value of the β -distribution derived using α and β , and σ is the square root of the variance. The posterior distributions of the mean and variance reveal clear differences between the metal-poor and metal-rich samples. The metal-rich group exhibits a larger average Δi and a broader Δi distribution, with $\mu = 3.13^{\circ}_{-0.49}^{+0.51}$ and $\sigma = 3.12^{\circ}_{-0.43}^{+0.43}$, compared to the metal-poor group, which has $\mu = 1.30^{\circ}_{-0.21}^{+0.20}$ and $\sigma = 1.00^{\circ}_{-0.19}^{+0.19}$.

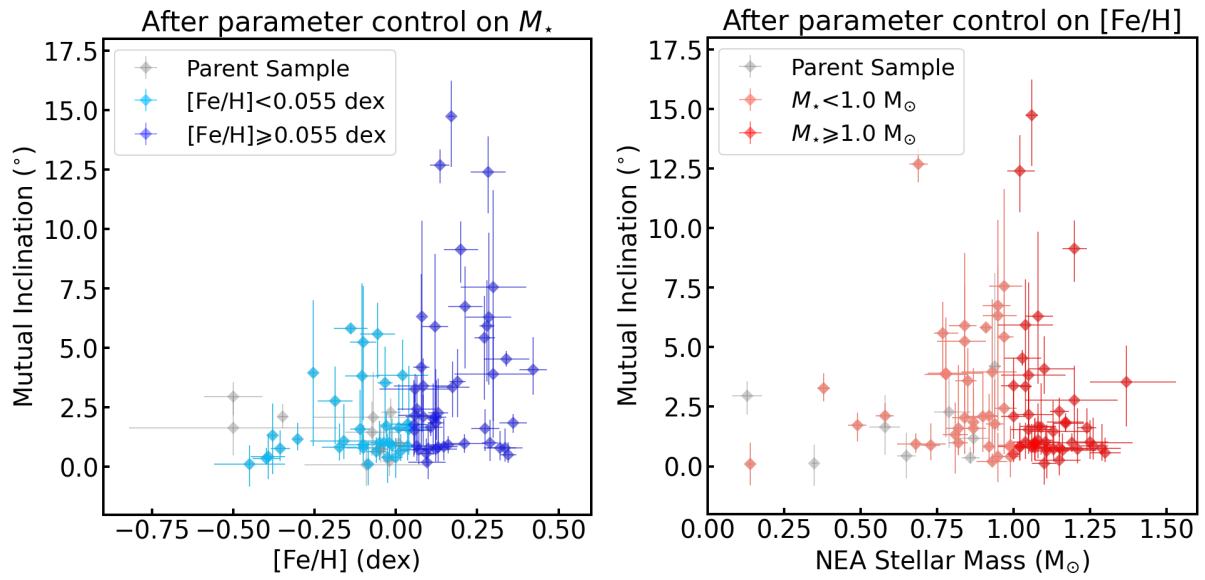


Figure 5. Relations between mutual inclination and stellar metallicity and stellar mass after sample control. Left: stellar metallicity vs. mutual inclination plot for a subsample of 78 systems selected to minimize the influence of stellar mass. Right: stellar mass vs. mutual inclination plot for a subsample of 81 systems selected to minimize the influence of stellar metallicity. Unlike $[\text{Fe}/\text{H}]$ vs. Δi , the correlation between stellar mass and Δi is not statistically significant in our sample, although we cannot completely rule out such a correlation. See Section 5 for more details.

REFERENCES

- An, D.-S., Xie, J.-W., Dai, Y.-Z., & Zhou, J.-L. 2023, *AJ*, 165, 125, doi: [10.3847/1538-3881/acb533](https://doi.org/10.3847/1538-3881/acb533)
- Anderson, S. G., Dittmann, J. A., Ballard, S., & Bedell, M. 2021, *AJ*, 161, 203, doi: [10.3847/1538-3881/abe70b](https://doi.org/10.3847/1538-3881/abe70b)
- Becker, J., Batygin, K., Fabrycky, D., et al. 2020, *AJ*, 160, 254, doi: [10.3847/1538-3881/abbad3](https://doi.org/10.3847/1538-3881/abbad3)
- Becker, J. C., & Adams, F. C. 2017, *MNRAS*, 468, 549, doi: [10.1093/mnras/stx461](https://doi.org/10.1093/mnras/stx461)
- Bensby, T., Feltzing, S., & Oey, M. S. 2014, *A&A*, 562, A71, doi: [10.1051/0004-6361/201322631](https://doi.org/10.1051/0004-6361/201322631)
- Bonfanti, A., Brady, M., Wilson, T. G., et al. 2024, *A&A*, 682, A66, doi: [10.1051/0004-6361/202348180](https://doi.org/10.1051/0004-6361/202348180)
- Borucki, W. J., Koch, D., Basri, G., et al. 2010, *Science*, 327, 977, doi: [10.1126/science.1185402](https://doi.org/10.1126/science.1185402)
- Brefka, L., & Becker, J. C. 2021, *AJ*, 162, 242, doi: [10.3847/1538-3881/ac2a32](https://doi.org/10.3847/1538-3881/ac2a32)
- Brewer, J. M., Wang, S., Fischer, D. A., & Foreman-Mackey, D. 2018, *ApJL*, 867, L3, doi: [10.3847/2041-8213/aae710](https://doi.org/10.3847/2041-8213/aae710)
- Bryan, M. L., Knutson, H. A., Lee, E. J., et al. 2019, *AJ*, 157, 52, doi: [10.3847/1538-3881/aaf57f](https://doi.org/10.3847/1538-3881/aaf57f)
- Buchhave, L. A., Bitsch, B., Johansen, A., et al. 2018, *ApJ*, 856, 37, doi: [10.3847/1538-4357/aaafca](https://doi.org/10.3847/1538-4357/aaafca)
- Buchhave, L. A., Latham, D. W., Johansen, A., et al. 2012, *Nature*, 486, 375, doi: [10.1038/nature11121](https://doi.org/10.1038/nature11121)
- Buchner, J. 2016, *Statistics and Computing*, 26, 383, doi: [10.1007/s11222-014-9512-y](https://doi.org/10.1007/s11222-014-9512-y)
- . 2019, *PASP*, 131, 108005, doi: [10.1088/1538-3873/aae7fc](https://doi.org/10.1088/1538-3873/aae7fc)
- . 2021, *The Journal of Open Source Software*, 6, 3001, doi: [10.21105/joss.03001](https://doi.org/10.21105/joss.03001)
- Buchner, J., Georgakakis, A., Nandra, K., et al. 2014, *A&A*, 564, A125, doi: [10.1051/0004-6361/201322971](https://doi.org/10.1051/0004-6361/201322971)
- Chen, D.-C., Xie, J.-W., Zhou, J.-L., et al. 2021, *ApJ*, 909, 115, doi: [10.3847/1538-4357/abd5be](https://doi.org/10.3847/1538-4357/abd5be)
- . 2023, *Proceedings of the National Academy of Science*, 120, e2304179120, doi: [10.1073/pnas.2304179120](https://doi.org/10.1073/pnas.2304179120)
- Cui, X.-Q., Zhao, Y.-H., Chu, Y.-Q., et al. 2012, *Research in Astronomy and Astrophysics*, 12, 1197, doi: [10.1088/1674-4527/12/9/003](https://doi.org/10.1088/1674-4527/12/9/003)
- Dai, F., Masuda, K., & Winn, J. N. 2018, *ApJL*, 864, L38, doi: [10.3847/2041-8213/aadd4f](https://doi.org/10.3847/2041-8213/aadd4f)
- Dawson, R. I., & Murray-Clay, R. A. 2013, *ApJL*, 767, L24, doi: [10.1088/2041-8205/767/2/L24](https://doi.org/10.1088/2041-8205/767/2/L24)
- Drążkowska, J., Bitsch, B., Lambrechts, M., et al. 2023, in *Astronomical Society of the Pacific Conference Series*, Vol. 534, *Protostars and Planets VII*, ed. S. Inutsuka, Y. Aikawa, T. Muto, K. Tomida, & M. Tamura, 717, doi: [10.48550/arXiv.2203.09759](https://doi.org/10.48550/arXiv.2203.09759)
- Espinoza, N., Kossakowski, D., & Brahm, R. 2019, *MNRAS*, 490, 2262, doi: [10.1093/mnras/stz2688](https://doi.org/10.1093/mnras/stz2688)
- Faridani, T., Naoz, S., Li, G., Rice, M., & Inzunza, N. 2024, *arXiv e-prints*, arXiv:2406.09359, doi: [10.48550/arXiv.2406.09359](https://doi.org/10.48550/arXiv.2406.09359)
- Fischer, D. A., & Valenti, J. 2005, *ApJ*, 622, 1102, doi: [10.1086/428383](https://doi.org/10.1086/428383)
- Guerrero, N. M., Seager, S., Huang, C. X., et al. 2021, *ApJS*, 254, 39, doi: [10.3847/1538-4365/abef1](https://doi.org/10.3847/1538-4365/abef1)
- Hansen, B. M. S., & Murray, N. 2013, *ApJ*, 775, 53, doi: [10.1088/0004-637X/775/1/53](https://doi.org/10.1088/0004-637X/775/1/53)
- Holtzman, J. A., Hasselquist, S., Shetrone, M., et al. 2018, *AJ*, 156, 125, doi: [10.3847/1538-3881/aad4f9](https://doi.org/10.3847/1538-3881/aad4f9)
- Huang, Y., Beers, T. C., Wolf, C., et al. 2022, *ApJ*, 925, 164, doi: [10.3847/1538-4357/ac21cb](https://doi.org/10.3847/1538-4357/ac21cb)
- Ida, S., & Lin, D. N. C. 2008, *ApJ*, 673, 487, doi: [10.1086/523754](https://doi.org/10.1086/523754)
- Izidoro, A., Bitsch, B., Raymond, S. N., et al. 2021, *A&A*, 650, A152, doi: [10.1051/0004-6361/201935336](https://doi.org/10.1051/0004-6361/201935336)
- Izidoro, A., Ogihara, M., Raymond, S. N., et al. 2017, *MNRAS*, 470, 1750, doi: [10.1093/mnras/stx1232](https://doi.org/10.1093/mnras/stx1232)
- Jenkins, J. M., Twicken, J. D., McCauliff, S., et al. 2016, in *Society of Photo-Optical Instrumentation Engineers (SPIE) Conference Series*, Vol. 9913, *Software and Cyberinfrastructure for Astronomy IV*, ed. G. Chiozzi & J. C. Guzman, 99133E, doi: [10.1117/12.2233418](https://doi.org/10.1117/12.2233418)
- Johnson, J. A., Aller, K. M., Howard, A. W., & Crepp, J. R. 2010, *PASP*, 122, 905, doi: [10.1086/655775](https://doi.org/10.1086/655775)
- Lai, D., & Pu, B. 2017, *AJ*, 153, 42, doi: [10.3847/1538-3881/153/1/42](https://doi.org/10.3847/1538-3881/153/1/42)
- Lam, K. W. F., Cabrera, J., Hooton, M. J., et al. 2023, *MNRAS*, 519, 1437, doi: [10.1093/mnras/stac3639](https://doi.org/10.1093/mnras/stac3639)
- Lambrechts, M., Morbidelli, A., Jacobson, S. A., et al. 2019, *A&A*, 627, A83, doi: [10.1051/0004-6361/201834229](https://doi.org/10.1051/0004-6361/201834229)
- Lightkurve Collaboration, Cardoso, J. V. d. M., Hedges, C., et al. 2018, *Lightkurve: Kepler and TESS time series analysis in Python*, *Astrophysics Source Code Library*. <http://ascl.net/1812.013>
- Lissauer, J. J., Ragozzine, D., Fabrycky, D. C., et al. 2011, *ApJS*, 197, 8, doi: [10.1088/0067-0049/197/1/8](https://doi.org/10.1088/0067-0049/197/1/8)
- Mann, A. W., Dupuy, T., Muirhead, P. S., et al. 2017, *AJ*, 153, 267, doi: [10.3847/1538-3881/aa7140](https://doi.org/10.3847/1538-3881/aa7140)
- Mann, H. B., & Whitney, D. R. 1947, *The Annals of Mathematical Statistics*, 18, 50, doi: [10.1214/aoms/1177730491](https://doi.org/10.1214/aoms/1177730491)
- Millholland, S., Wang, S., & Laughlin, G. 2017, *ApJL*, 849, L33, doi: [10.3847/2041-8213/aa9714](https://doi.org/10.3847/2041-8213/aa9714)
- Millholland, S. C., He, M. Y., Ford, E. B., et al. 2021, *AJ*, 162, 166, doi: [10.3847/1538-3881/ac0f7a](https://doi.org/10.3847/1538-3881/ac0f7a)

- Mills, S. M., Howard, A. W., Petigura, E. A., et al. 2019, *AJ*, 157, 198, doi: [10.3847/1538-3881/ab1009](https://doi.org/10.3847/1538-3881/ab1009)
- Mordasini, C., Alibert, Y., Klahr, H., & Henning, T. 2012, *A&A*, 547, A111, doi: [10.1051/0004-6361/201118457](https://doi.org/10.1051/0004-6361/201118457)
- Moriarty, J., & Ballard, S. 2016, *ApJ*, 832, 34, doi: [10.3847/0004-637X/832/1/34](https://doi.org/10.3847/0004-637X/832/1/34)
- Morton, T. D., Bryson, S. T., Coughlin, J. L., et al. 2016, *ApJ*, 822, 86, doi: [10.3847/0004-637X/822/2/86](https://doi.org/10.3847/0004-637X/822/2/86)
- Mulders, G. D., Pascucci, I., Apai, D., Frasca, A., & Molenda-Żakowicz, J. 2016, *AJ*, 152, 187, doi: [10.3847/0004-6256/152/6/187](https://doi.org/10.3847/0004-6256/152/6/187)
- Mustill, A. J., Davies, M. B., & Johansen, A. 2017, *MNRAS*, 468, 3000, doi: [10.1093/mnras/stx693](https://doi.org/10.1093/mnras/stx693)
- Ndugu, N., Bitsch, B., & Jurua, E. 2018, *MNRAS*, 474, 886, doi: [10.1093/mnras/stx2815](https://doi.org/10.1093/mnras/stx2815)
- Peterson, M. S., Benneke, B., Collins, K., et al. 2023, *Nature*, 617, 701, doi: [10.1038/s41586-023-05934-8](https://doi.org/10.1038/s41586-023-05934-8)
- Petigura, E. A., Marcy, G. W., Winn, J. N., et al. 2018, *AJ*, 155, 89, doi: [10.3847/1538-3881/aaa54c](https://doi.org/10.3847/1538-3881/aaa54c)
- Petrovich, C., Deibert, E., & Wu, Y. 2019, *AJ*, 157, 180, doi: [10.3847/1538-3881/ab0e0a](https://doi.org/10.3847/1538-3881/ab0e0a)
- Pu, B., & Lai, D. 2018, *MNRAS*, 478, 197, doi: [10.1093/mnras/sty1098](https://doi.org/10.1093/mnras/sty1098)
- . 2019, *MNRAS*, 488, 3568, doi: [10.1093/mnras/stz1817](https://doi.org/10.1093/mnras/stz1817)
- . 2021, *MNRAS*, 508, 597, doi: [10.1093/mnras/stab2504](https://doi.org/10.1093/mnras/stab2504)
- Ricker, G. R., Winn, J. N., Vanderspek, R., et al. 2015, *Journal of Astronomical Telescopes, Instruments, and Systems*, 1, 014003, doi: [10.1117/1.JATIS.1.1.014003](https://doi.org/10.1117/1.JATIS.1.1.014003)
- Smith, J. C., Stumpe, M. C., Van Cleve, J. E., et al. 2012, *PASP*, 124, 1000, doi: [10.1086/667697](https://doi.org/10.1086/667697)
- Soubiran, C., Le Campion, J.-F., Brouillet, N., & Chemin, L. 2016, *A&A*, 591, A118, doi: [10.1051/0004-6361/201628497](https://doi.org/10.1051/0004-6361/201628497)
- Sousa, S. G., Adibekyan, V., Delgado-Mena, E., et al. 2021, *A&A*, 656, A53, doi: [10.1051/0004-6361/202141584](https://doi.org/10.1051/0004-6361/202141584)
- Spalding, C., & Batygin, K. 2016, *ApJ*, 830, 5, doi: [10.3847/0004-637X/830/1/5](https://doi.org/10.3847/0004-637X/830/1/5)
- Speagle, J. S. 2019, arXiv e-prints, arXiv:1904.02180, <https://arxiv.org/abs/1904.02180>
- Stumpe, M. C., Smith, J. C., Catanzarite, J. H., et al. 2014, *PASP*, 126, 100, doi: [10.1086/674989](https://doi.org/10.1086/674989)
- Stumpe, M. C., Smith, J. C., Van Cleve, J. E., et al. 2012, *PASP*, 124, 985, doi: [10.1086/667698](https://doi.org/10.1086/667698)
- Wang, J., & Fischer, D. A. 2015, *AJ*, 149, 14, doi: [10.1088/0004-6256/149/1/14](https://doi.org/10.1088/0004-6256/149/1/14)
- Weiss, L. M., Marcy, G. W., Petigura, E. A., et al. 2018, *AJ*, 155, 48, doi: [10.3847/1538-3881/aa9ff6](https://doi.org/10.3847/1538-3881/aa9ff6)
- Winn, J. N., Sanchis-Ojeda, R., Rogers, L., et al. 2017, *AJ*, 154, 60, doi: [10.3847/1538-3881/aa7b7c](https://doi.org/10.3847/1538-3881/aa7b7c)
- Xie, J.-W., Dong, S., Zhu, Z., et al. 2016, *Proceedings of the National Academy of Science*, 113, 11431, doi: [10.1073/pnas.1604692113](https://doi.org/10.1073/pnas.1604692113)
- Yang, J.-Y., Chen, D.-C., Xie, J.-W., et al. 2023, *AJ*, 166, 243, doi: [10.3847/1538-3881/ad0368](https://doi.org/10.3847/1538-3881/ad0368)
- Zanazzi, J. J., & Lai, D. 2018, *MNRAS*, 478, 835, doi: [10.1093/mnras/sty1075](https://doi.org/10.1093/mnras/sty1075)
- Zhou, J.-L., Lin, D. N. C., & Sun, Y.-S. 2007, *ApJ*, 666, 423, doi: [10.1086/519918](https://doi.org/10.1086/519918)
- Zhu, W. 2019, *ApJ*, 873, 8, doi: [10.3847/1538-4357/ab0205](https://doi.org/10.3847/1538-4357/ab0205)
- . 2024, *Research in Astronomy and Astrophysics*, 24, 045013, doi: [10.1088/1674-4527/ad3132](https://doi.org/10.1088/1674-4527/ad3132)
- Zhu, W., & Dong, S. 2021, *ARA&A*, 59, 291, doi: [10.1146/annurev-astro-112420-020055](https://doi.org/10.1146/annurev-astro-112420-020055)
- Zhu, W., Petrovich, C., Wu, Y., Dong, S., & Xie, J. 2018, *ApJ*, 860, 101, doi: [10.3847/1538-4357/aac6d5](https://doi.org/10.3847/1538-4357/aac6d5)